Detecting oil in sea ice using Ground-penetrating radar: Developing a new airborne system

2012 CRREL Test Report

DICKINS **AlloSys Corporation** **BOISE STATE UNIVERSITY**

March 2012

THIS PAGE BLANK ON PURPOSE

Detecting oil in sea ice using Ground-penetrating radar: Developing a new airborne system

2012 CRREL Test Report

March 31, 2012

Prepared for:

Joint Industry Project Participants

Submitted by:

DF Dickins Associates, LLC
David Dickins
dfdickins@sbcglobal.net

Boise State University (CGISS)
Hans Peter Marshall
hpmarshall@boisestate.edu

AllosSys Corporation
Robert Hay
bob@allosys.com

ACKNOWLEDGEMENTS

PARTICIPANTS

The following participants fund this Joint Industry Project:

- Alaska Clean Seas
- Bureau of Safety and Environmental Enforcement (BSEE)
- ConocoPhillips
- ExxonMobil Upstream Research Company
- Shell International Exploration and Production
- Statoil Petroleum

Summary, Conclusions and Recommendations

The second prototype of a new FMCW airborne radar system was tested February 7 and 8 over 37-46 cm of sea ice grown in the same outdoor basin at the CRREL facility in Hanover NH as used for the initial tests in 2011.   This report summarizes the state of knowledge and evolution of the recent radar development program initiated in late 2009 and provides detailed results from analysis and interpretation of the 2012 data.

Oil was spilled into an ~5 cm under ice depression created by adding extra insulation to a 3 m^2 area part way through the ice growth phase. Two oil discharges were completed totaling 63 US gal (0.23 m^3), the first filling the depression partially to an estimated average oil thickness of 2 cm, and the second filling the depression to overflowing, resulting in average and maximum estimated oil layer depths of 4 and 7 cm respectively. Cores were taken to document ice salinity and temperature and to determine the extent of any vertical oil migration over the two-day test period. The ice sheet was very warm (within 2°C of the melting point), which has major implications in terms of the degree of signal attenuation and amount of radar energy than can penetrate to the ice/water interface. The high ice conductivity led to very severe test conditions.

The second prototype airborne radar system was tested in a number of different orientations and heights above the ice, including stationary sampling and profiles run from the moving gantry laterally and longitudinally over the oiled area.

The data collected at CRREL in 2012 provides useful insight into the radar characteristics of the ice and supports the hypothesis that the ice sheet grown in the basin was a material that reflected the radar waves throughout its thickness. This is consistent with the observation that it is difficult for a radar signal to penetrate reasonably warm saline ice. Despite the challenging conditions, there is reason to believe that the new system was able to provide some penetration, to potentially detect the bottom of the ice, and possibly even to be affected by the presence of oil under the surface. The 2012 test program with the second prototype FMCW system (reported here) confirmed the previous findings with warm ice sheets (e.g. Svalbard 2006), that GPR systems are unlikely to provide reliable detection of oil in or under ice once the internal temperatures are close to the melting point.

In order to achieve the wide tuning range in the second FMCW prototype system, it was necessary to use a heterodyne source with two oscillators. Any heterodyne system will produce spurious mixing products, and with the first design chosen due to various time and budget constraints, these spurious products were higher than desirable. As a result, there are numerous artifacts in the data showing reflections where there should not be any. These did not cause any problems in the current analysis because the areas of interest were well known and consequently, the spurious responses could be neglected. That would not be the case for more general analysis of field data where the user lacked the benefit of prior knowledge of the oil whereabouts and ice characteristics. A separate proposal submitted (4/12) describes a number of design improvements that should eliminate much of the spurious signal content encountered in the latest tests.

The radar system functioned very well except for the spurious responses described. The very low phase noise and excellent linearity, due to the use of high-quality oscillators and a newly designed Phase Locked Look by Analog Devices led to some excellent results under difficult conditions. The use of the Low Noise Amplifier directly connected to the receive antenna provided for an excellent system noise figure. Despite the very high attenuation of the warm saline ice, it is apparent that the Signal to Noise Ratio (SNR) of the system was adequate to receive a signal that penetrated even the warm ice.

The utility of the system could be significantly enhanced by developing a third prototype with improvements based on what was learned from the CRREL experience. For example, increasing oscillator frequencies and reducing levels at critical mixers will serve to both increase the order of the spurious products reduce their magnitude, moving them further from frequency and amplitude regions where they can cause spurious responses. Further increases in the SN ratio anticipated in the next design evolution could increase the possibility of penetrating the ice sheet over a wider range of temperature conditions.

It is also clear from the latest CRREL experience that a much better understanding of the signatures of ice and oil would benefit from further controlled research in a cold room. The CRREL ice sheet reflection profile was quite different from what was expected. It is important to understand how this profile might vary for ice at different temperatures and salinity levels. One key question relates to the assumption that oil is detectable with GPR because of its homogeneous properties, such that radar reflections are negligible within the oil layer while occurring only at the interfaces? A much better understanding of these critical issues could be developed using a well-controlled environment such as that found at the new Boise State BSU Cryosphere Geophysics and Remote Sensing (CryoGARS) Laboratories (refer to separate proposal).

Table of contents   page

1.   Background

1.1 State of Knowledge

The current state of knowledge surrounding GPR capabilities for oil-in-ice detection, based on all the testing over the past eight years is summarized briefly as follows:

- Previous tank testing at CRREL (2004) and in field tests in Norway (2006) demonstrated that a surface-based ground-penetrating radar (GPR) operating at 500 MHz to 1GHz can clearly delineate changes at the ice water interface caused by emplacement of oil.
- Testing at CRREL in March 2011 (described in the 2011 Field Report and 2010/11 Program summary) showed that the commercially available impulse GPR operated from the ice surface and up to a height of ~3 m is capable of differentiating oiled from clean ice under freezing conditions with relatively cold ice sheets. *Note: Previous attempts to fly this unit at low altitude (5-10 m) in Norway in 2006 showed that it was incapable of profiling the ice undersurface or detecting oil with a relatively warm ice sheet.*
- The existing, portable commercial GPR systems are capable of profiling natural sea ice sheets from the surface at least as thick as 2 m as late as April (warmer ice later in the ice season could reduce the allowable thickness). This claim is based on the results of the April 2005 trials with ACS at Prudhoe Bay.
- The 2012 test program with the second prototype FMCW system (reported here) confirmed the previous findings with warm ice sheets (e.g. Svalbard 2006), that GPR systems are unlikely to provide reliable detection of oil in or under ice once the internal temperatures are close to the melting point.

1.2 Overview of the Airborne Radar Design, Development and Testing:

Initiated in late 2009, the current oil-in-ice Ground Penetrating Radar (GPR) project differs from the previous work in this field by focusing on new hardware development to design and fabricate prototype, higher-powered and more directional radar systems that can be used operationally to detect oil under sea ice from a low-flying helicopter.

The new system operates in a frequency range optimized for measuring oil under sea ice with antennae designed to greatly increase the directionality of the transmitted signal. Due to the RF absorption of saline ice, it was determined that the upper frequency needed to be limited to 2 GHz. A lower frequency limit of 500 MHz was dictated largely by the bandwidth of horn antennas of a size and weight suitable for helicopter mounting.   A Frequency Modulated Continuous Wave (FMCW) architecture was selected to provide several clear benefits over the pulse radars previously tested, including:
- Avoiding the need to develop high-energy impulses associated with pulse radar,
- Using the maximum available spectrum to achieve the optimum resolution.

The hardware for the first prototype of the new radar design was completed in late 2010, capable of using either horn-based antennas, or a larger horn-fed reflector dish. At this stage, development is proceeding only with the horn-based antennas as the most likely system to reach flight status in the short term.

The test and development program over the past year incorporated three components:

1. Testing the first prototype in March 2011 with crude oil spilled underneath an artificially grown 92 cm thick ice sheet in large outdoor basin at the US Army Cold Regions Environmental Laboratory (CRREL). The radar was supported above the ice on a moving overhead gantry frame. Those results showed that further development work was needed to improve the signal to noise ratio of the new system (See 2.)
2. Development of an improved second prototype, incorporating hardware modifications based on results from the 2011 CRREL testing (the new system is described in detail in the 2010/11 Program Report submitted January 2012). ***Note: This step replaced flight trials at Prudhoe Bay, originally planned for early April 2011.***
3. Testing the second prototype in February 2012 with crude oil spilled under 45 cm of sea ice grown in the same outdoor tank as the previous year. Further design improvements and an incremental testing/development program in a cold room are proposed for the period May to December 2012 in place of planned Prudhoe Bay flight trials for the same year (Covered under a separate proposal submitted 4/03/12)

This report describes the test set up and findings from the most recent CRREL test program conducted February 6-9, 2012.

2. 2012 CRREL Test Program Overview

The tests completed at CRREL in 2012 consisted of manual up/down tests from the ice surface to a height of several meters, multiple scans of the pool in both axes from the moving gantry, and stationary testing over the region where oil was injected into an existing, artificially created depression in the ice over a 2-day period. The ice thickness ranged from 37 to 45 cm, and the temperature of the saline ice was within a few degrees of the freezing point of seawater (-1.8°C).

Conveniently, the commercial impulse GPR owned and operated by Alaska Clean Seas was used for training over a different section of the same ice sheet at colder temperatures. Those results provided a useful comparison and confirmed that the degradation in performance that the team experienced a week later with the FMCW system was tied to the increase in ice temperatures. This was also confirmed with subsequent computer modeling of expected signal attenuation under different scenarios prior to making the decision to cancel the 2012 Prudhoe testing. The modeling results indicated that the predicted signal amplitude with up to 2.2 m of sea ice possible at Prudhoe (after a record cold winter) would be comparable to that achieved with warm,

relatively thin ice on February 7, 2012 at CRREL. In other words, based on the CRREL data, there appeared to be little utility in proceeding with the Prudhoe trials this year.

In addition to the ongoing automatic monitoring of the ice temperature at different depths, CRREL staff also extracted two ice cores for salinity and temperature profiles and completed a pattern of two-inch drill holes to map the variations in ice thickness **(Fig. 6).**

The 2012 radar test layout, ice characteristics and results are summarized in the following Sections 3 and 4.

3. Test Layout and Ice Properties

3.1 Set-up and Oil Injection

The project utilized the Geophysical Research Facility at CRREL to develop a test sea ice sheet. This facility consists of a concrete basin, 18.25 m long × 6.7 m wide × 2 m deep (60 × 22 × 7 ft), with a removable roof that grows and maintains a growing ice cover in a refrigerated ambient environment and protects it from snow and rain

Most important for testing the radar systems in an "airborne" mode, was the fact that the tank incorporates a moving gantry that runs the full length of the basin on rails (**Fig. 1**). This provides a convenient mounting point for FMCW system **(Fig. 13).**

Figure 1. Test facility in 2012 showing the disturbed ice left from spill response training in the foreground and the North 1/3 of the basin reserved for radar testing behind the yellow skirt.

The test set-up differed from 2011 in that the radar team used only the North 1/3 of the tank shown in Fig. 1. Alaska Clean Seas responders utilized the remaining ice area for

Arctic oil spill recovery training the week prior to radar testing. A single skirt across the full tank width separated the two areas.

Oil was discharged through a pipe inserted through an angled augur hole to rise naturally under an artificially created depression in the ice (**Fig. 2**). This depression was created to satisfy the test requirements of an earlier program evaluating sonar to detect oil under ice in late January. By covering a 1.5 x 2m (approx) area with foam insulation part way through the growth process the ice thickness within the insulated was retarded to finish up to 8 cm thinner than the surrounding sheet (**Fig. 6**).

Figure 2.   View showing the curved discharge pipe subsequently inserted at an angle to project into the middle of the under ice depression marked in red spray paint.

3.2 Ice Properties: Salinity, Thickness and Temperature

Two cores were taken on each of the test days to document the ice salinity and temperature (**Figs. 3 to 5**)

Figure 3. Close up of the bottom of the core taken Feb. 7 showing the individual crystal platelets within the soft skeletal layer. The brown tint likely represents minor contamination through very fine dispersed droplets of oil spilled in the tank the week before.
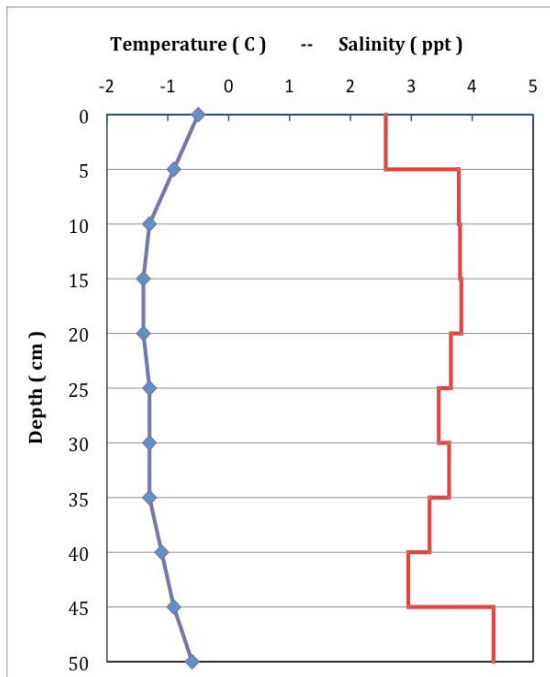

Figure 4. Temperature and salinity profiles from the first ice core taken close to the centerline of the basin, February 7, adjacent to the lateral skirt/curtain. Total ice thickness 50 cm, with a soft 4 cm bottom skeletal layer (**Fig. 3**). Water temperature in the slush-filled hole was -1.3°C.
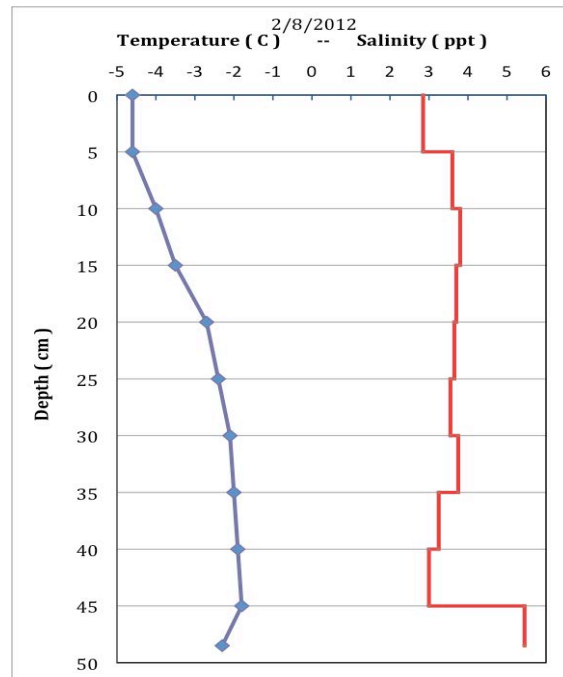
Figure 5. Temperature and salinity profiles from an ice core taken February 8 within 30 cm of the first core. Total ice thickness 48.5 cm, with a soft 2 cm bottom skeletal layer. Water temperature was -1.3°C (same as day previous).

3/31/12

Ice thickness was documented through a series of two-inch augur holes drilled at the end of testing (**Fig. 6**).
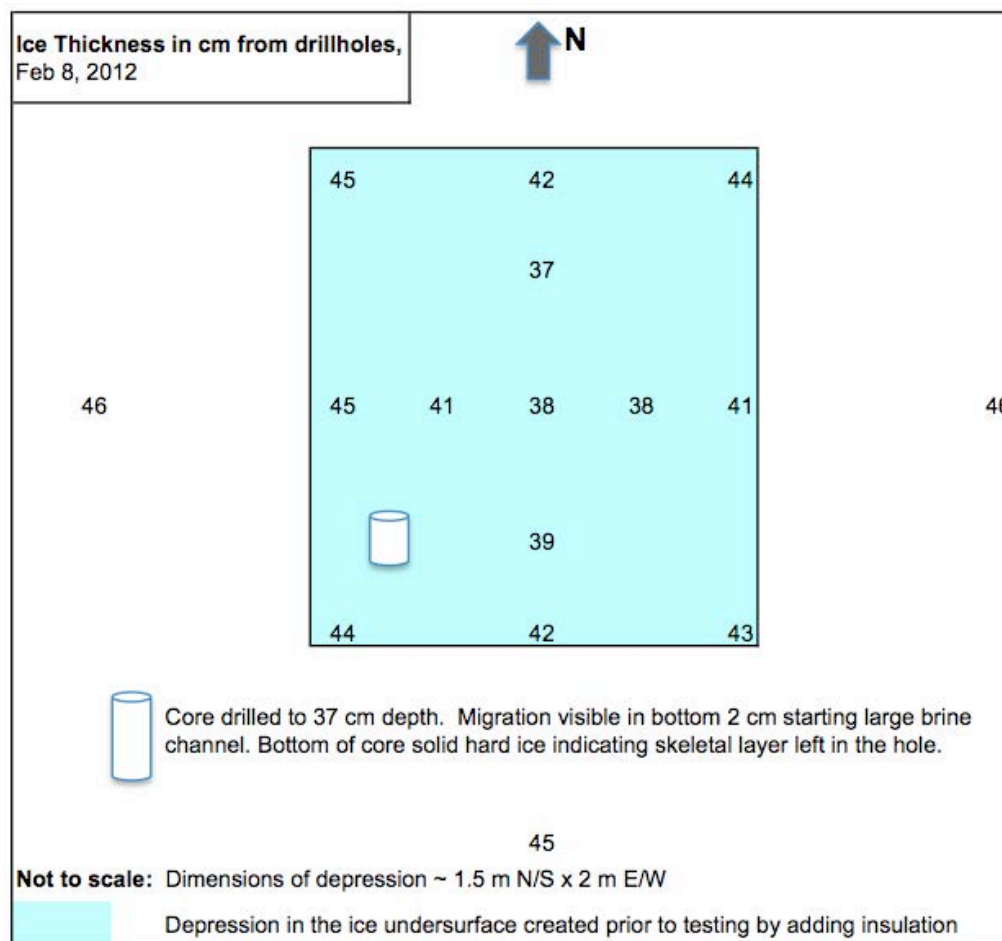

Ice Thickness in cm from drillholes, Feb 8, 2012

N

45   42   44

37

46   45   41   38   38   41   46

39

44   42   43

Core drilled to 37 cm depth. Migration visible in bottom 2 cm starting large brine channel. Bottom of core solid hard ice indicating skeletal layer left in the hole.

45

Not to scale: Dimensions of depression ~ 1.5 m N/S x 2 m E/W

Depression in the ice undersurface created prior to testing by adding insulation

Figure 6.   Diagram showing results from a series of augur holes drilled after testing to document the variability in ice thickness within the depression used to contain the oil and the undisturbed ice on the perimeter. This information was used to estimate and map the likely distribution and thickness of oil on the two test days (**Figs. 7and 8**).

3.3 Oil Film thickness and Distribution

Two spills were conducted, the first on February 7, partially filling the under ice depression documented through drilling (**Fig. 6**), and then completely filling the depression to just overflowing on February 8. The total volume spilled was 63 gal US (0.23 m^3). The determination of when the oil began to flow out of the depression, indicating the point of maximum oil thickness, was made with an upward looking underwater video camera. Estimates were made of oil thickness on both days by comparing the oil volume spilled with the total holding capacity of the depression mapped above (**Figs. 7 and 8 below**).
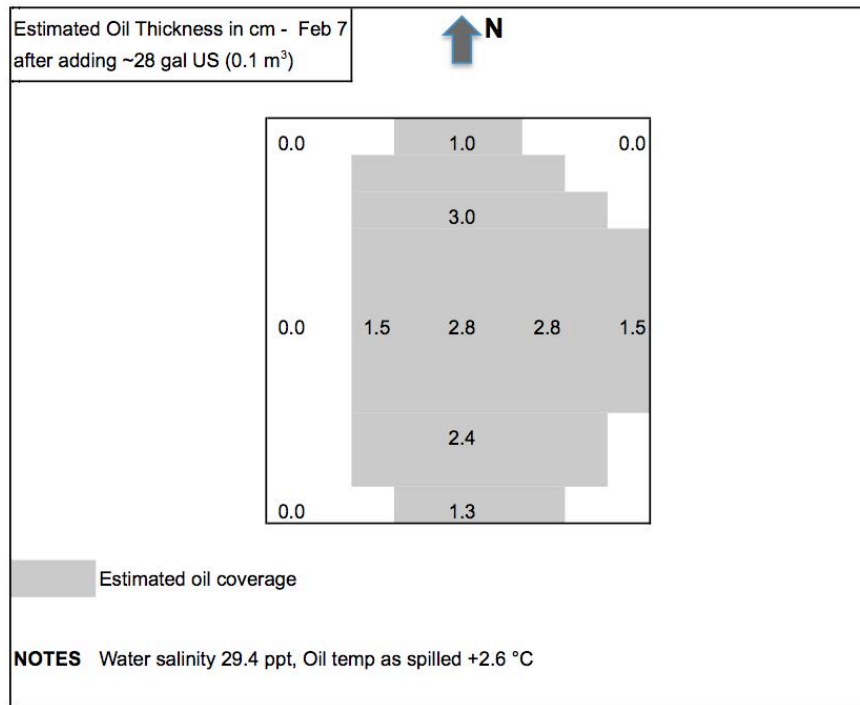
Estimated Oil Thickness in cm - Feb 7 after adding ~28 gal US (0.1 m³)

		0.0		1.0		0.0
				3.0		
0.0	1.5	2.8	2.8	1.5
				2.4		
		0.0		1.3		

Estimated oil coverage

NOTES Water salinity 29.4 ppt, Oil temp as spilled +2.6 °C

Figure 7. Oil pool thickness estimated for February 7 from ice thickness and oil volume.

Estimated Oil Thickness in cm - Feb 8 after adding additional 35 gal US (0.13 m³). Total oil volume added = 0.23 m³

		0.0		2.5		1.0
				7.0		
0.0	3.5	6.5	6.5	3.5
				5.5		
		1.0		3.0		1.5

NOTE   Oil temp as spilled +0.6 °C
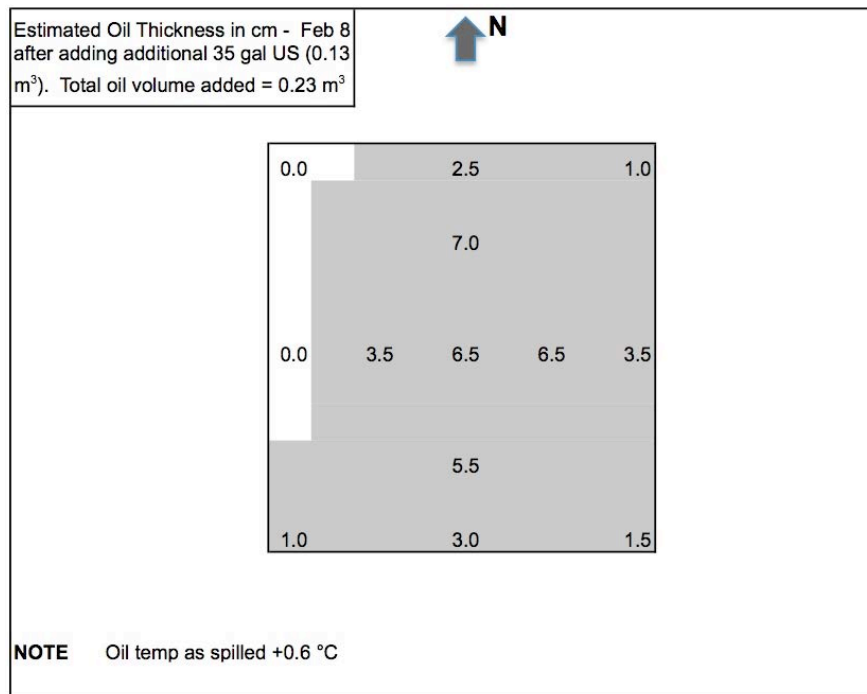
Figure 8. Corresponding oil thickness estimates for February 8.

As noted in Figure 7, a third core was taken within the oiled area after testing was complete (**Fig. 9**). This core was drilled to a depth of 37 cm within the ice depression (orange boundary in photographs) at a point with estimated ice thickness in the range of 41-42 cm. The purpose here was to investigate the extent of vertical oil migration without penetrating the oil and coating the core with oil in the hole. By not penetrating the full sheet it was possible retrieve a clean core for photography (**Fig. 10**).
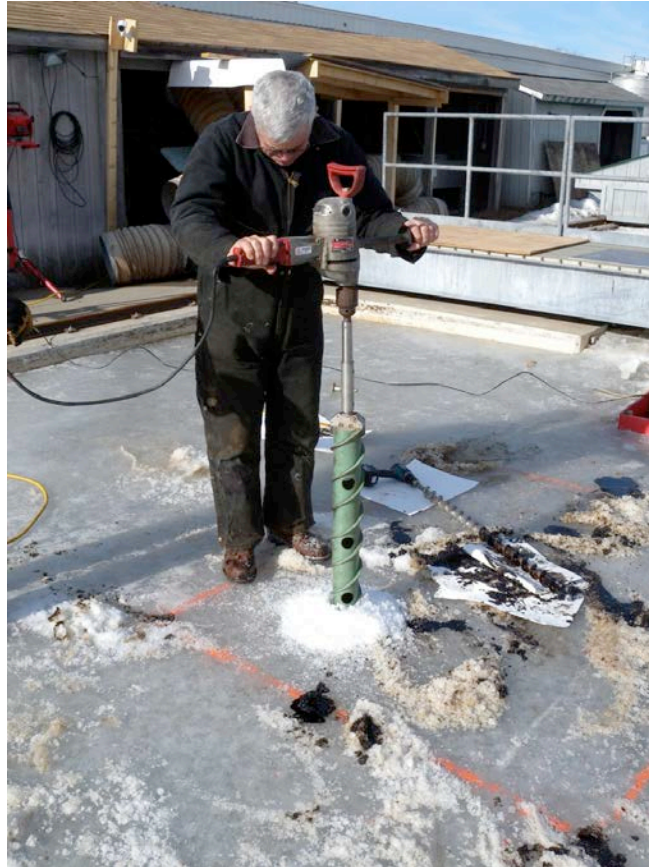
Figure 9. Coring within the oiled area to document any evidence of vertical oil migration.

Figure 10 shows the 37 cm partial core extracted on February 8 from above the oil filled ice depression. Oil filled brine channels are visible to a height of 2 cm above the bottom of the core where it broke off just above the skeletal layer left in place. This means that the oil saturated the bottom 2-4 cm of porous crystals (Fig. 3) and penetrated several cm into broad brine channels at the base of the hard ice.

Figure 10. Ice core, 37 cm taken Feb 8 within the oiled area, showing 2 cm migration into the base of the hard ice. An estimated 3-4 cm of soft skeletal layer was left intact at the bottom of the core hole.

4. Radar Results

Table 1 summarizes the radar test specifications and conditions.

Table 1

Radar System Used	FMCW prototype 1, built by AlloSys for BSU in 2011
Frequency range	500 MHz – 2 GHz → BW = 1.5e9 Hz
Frequency sweep	Linear triangular, 10 ms up, 10 ms down
Output power	Nominal 24 dBm (.25 watt)
Receiver	Quadrature, approx. 6 dB noise figure
Assumed ε_R	4.5 → v=1.414e10 cm/s
Resolution	v/2BW = 4.71 cm
Distance reference	Approximately at bottom of horns

The tests on February 7 and 8 consisted of manual up/down tests (**Fig. 11**), multiple scans over the oiled area in both axes from the gantry (**Fig. 12**), and stationary testing over the region where oil was injected over a 2-day period (**Fig. 13**). Results from these different tests are shown below in (**Figs. 14 to 22**).

Figure 11. Looking at signal differences with height above the ice.
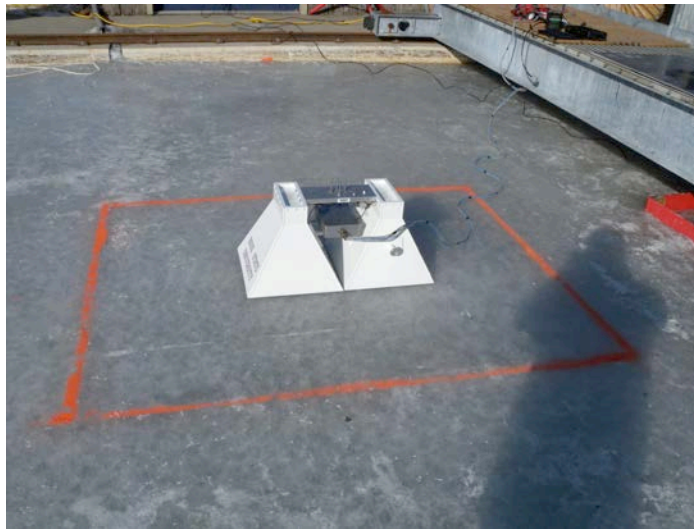
Figure 12. Horn antennae on the ice surface with the oiled area outlined in orange.

Figure 13. FMCW system mounted on sliding track under the moving gantry, allowing profiles N/S and E/W over the oiled area. In addition, the measurements were repeated with the system rotated 90 degrees to account for any effects due to ice anisotropy (preferred crystal alignment).

This discussion begins with results some of the up/down testing that was done to determine the ability of the radar system to characterize the ice. This turns out to be a very useful test because it allows for the characterization of artifacts by whether they move with the top of ice or are fixed relative to the antenna system.

Because of the use of a quadrature receiver, it was possible to derive the phase of the reflected signal by characterizing the magnitude of the in-phase and the quadrature signals. This analysis will look at both the magnitude and phase of the reflected signal, and explore ways they might be used synergistically.

It will also consider independently the response to both the downward and upward frequency transitions. While these produced similar results, they were not necessarily identical. Normally, any difference between these two transitions would be attributed to the Doppler effect due to a time-varying distance between the radar and the target. In this experiment these velocities were negligible, so in this case the difference is likely due to a minor difference in the ramp time of the two parts of the triangle ramp. Beginning with the magnitude response of an up/down test, the results are shown in Figure 14 and Figure 15.
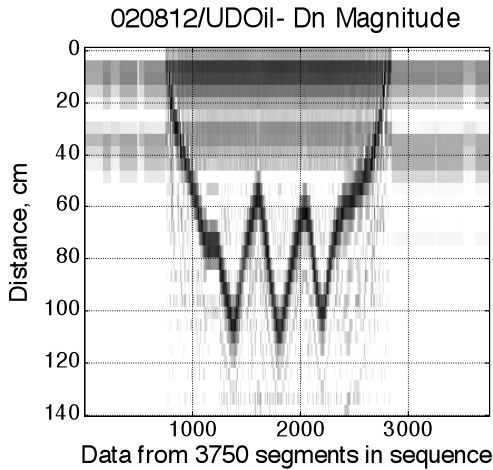
Figure 14. Down Magnitude
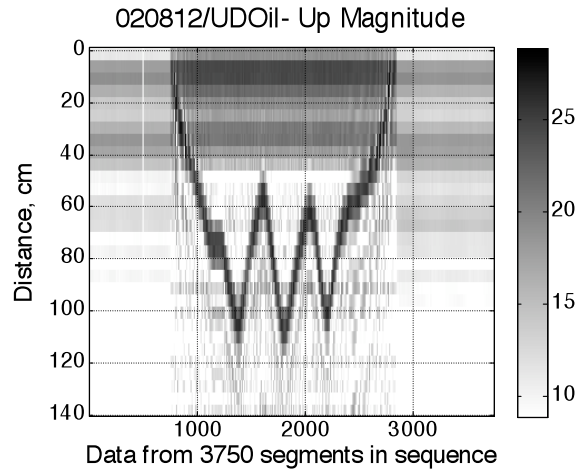
Figure 15. Up Magnitude

These results can be analyzed by doing a vertical autocorrelation to determine the correlation between the strong surface reflection and any subsurface reflection that occurs a fixed distance below the surface. The results of doing this autocorrelation in the region of interest, between segments 800 and 2700, and taking the mean of these autocorrelations across all columns, are shown as the solid blue lines in Figures 16 and 17. In these figures, the dashed red line (faintly visible) is a third-order best-fit approximation of the autocorrelation.
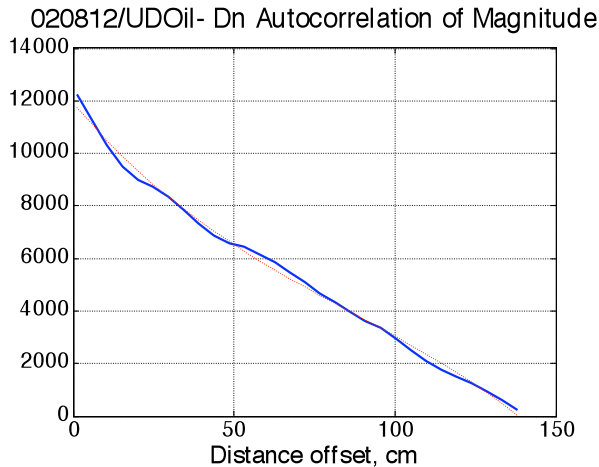
Figure 16. Down Magnitude Autocorrelation
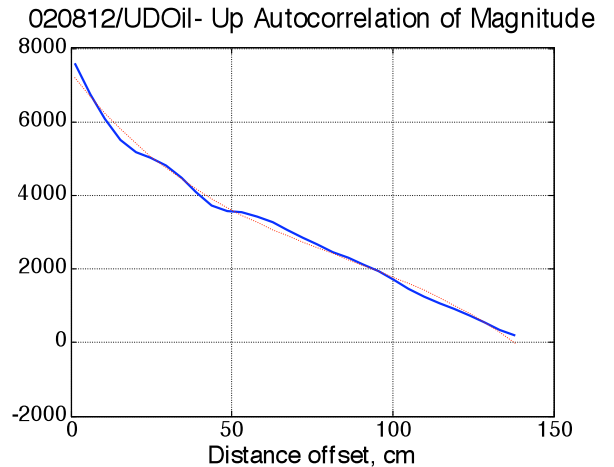
Figure 17. Up Magnitude Autocorrelation

The relatively high but declining level of the autocorrelation signal suggests that there is an ongoing reflection as the signal passes through the ice. This will be discussed more later. The short-term variation in the autocorrelation can be better seen by subtracting the polynomial approximation of the data and viewing the remainder. This result is shown in Figures 18 and 19. In both of these figures there is a distinct peak at 30 cm offset. While the signal is rather weak, as expected due to the attenuation of the ice, this

suggests a significant subsurface reflection closely associated with the ice surface. As will be discussed at the end of this paper, it is believed that the response seen in the vicinity of 60 cm is due to some signal characteristics that could be significantly reduced with some improvements proposed for the next generation of the radar system.
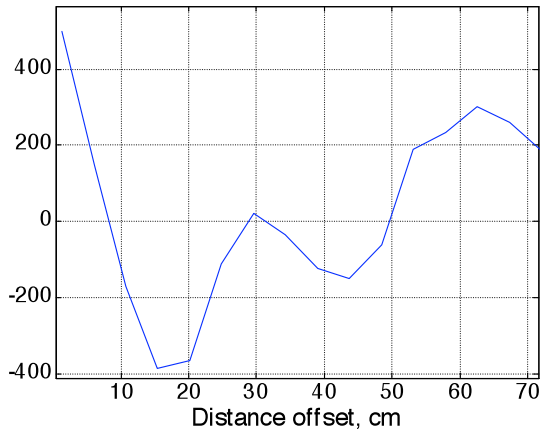

Figure 18. Down Autocorrelation Variation
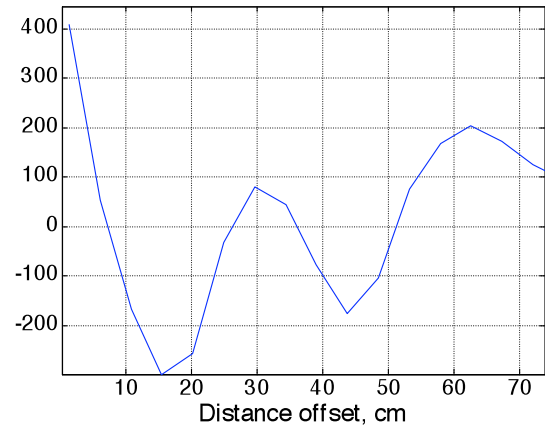
Figure 19. Up Autocorrelation Variation

The results of this up/down test provide an additional piece of useful information.   One concern remains the uncertainty caused by known side lobes of the antenna polar response. Any antenna will have side lobes, and these are exacerbated by size constraints. These side lobes can cause a reflection from the ice surface that appears to have a longer travel distance than the main lobe and can masquerade as subsurface reflections. In the case of the up/down test, the effective differential distance of these signals from these side lobes would be proportional to the distance between the antenna and the surface, so would not appear as a constant offset from the surface as would an actual subsurface reflection. Thus this notable distinct peak at 30 cm is an encouraging indication that it is the result of an actual subsurface reflection.

As noted, the benefit of having a quadrature receiver is that it facilitates computing the phase of the received signal and, in addition, assures that all frequency components are received independent of their phase shift. Phase data can be processed in a variety of ways. In this case, one of the more useful ways is to subtract the expected linear phase shift based on distance (and frequency), then to find the derivative of that difference. In regions where there is not much reflection, the phase data are relatively meaningless, and one approach is to use a reflection magnitude threshold to mask the phase data. Here that masking is not done so that the phase signal is visible for all ranges. There is an observation that can be made about the signal being reflected as it passes through the ice. It can be observed that the reflection is not necessarily dominated by a surface reflection, but rather appears to be a continual reflection as it passes through the ice. That may be a property of this particular ice sheet and its rather warm temperature. With this ice sheet, it is possible that it is not very homogeneous, with pockets of water and structural properties that cause reflections as the signal passes through the ice. It

also appears that the reflected phase as the signal passes through the ice is relatively consistent with what would be expected given the assumed phase velocity of the ice. Consequently, it can be seen that the differential phase in the region of the ice sheet shows very low phase shift as indicated by the light coloration in that region in Figures 20 and 21. In these figures, it is apparent that this region of constant phase response indicated by the light-colored region is on the order of the expected ice thickness. Note that the color selection for these plots reflects the notion that phase is a rotation, and the color at +pi and –pi radians should be the same as they are identical
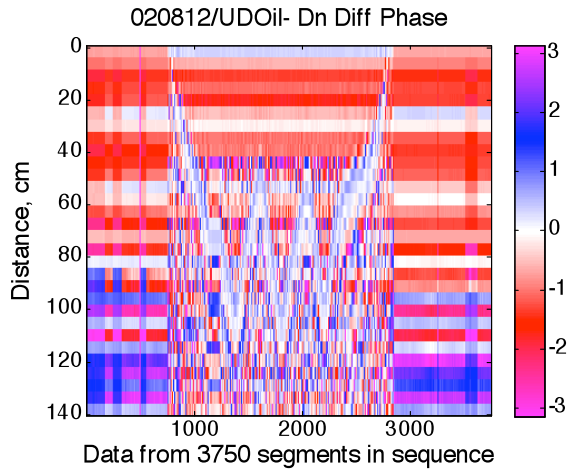
Figure 20. Down Reflected Differential Phase (radians)
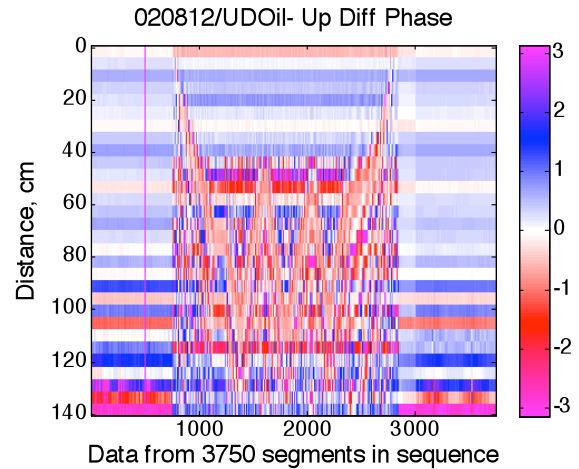
Figure 21. Up Reflected Differential Phase (radians)

It is reasonable to question why these results suggest the ice sheet is around 30 cm thick when the core sample indicated that it was around 40 cm thick. To explore that question further, consider the results of the shovel test, where a shovel was slowly lowered from the antenna pair to a position where it was resting on the top of the ice sheet.
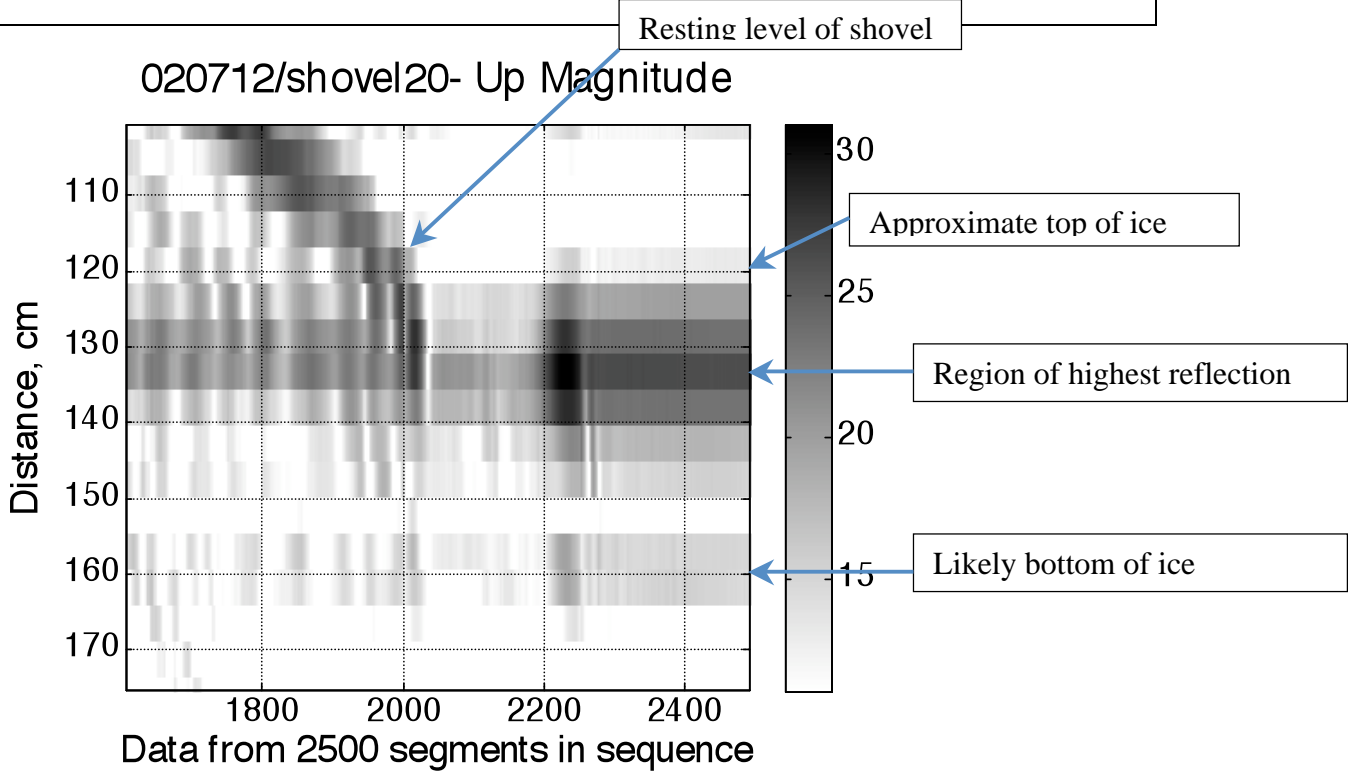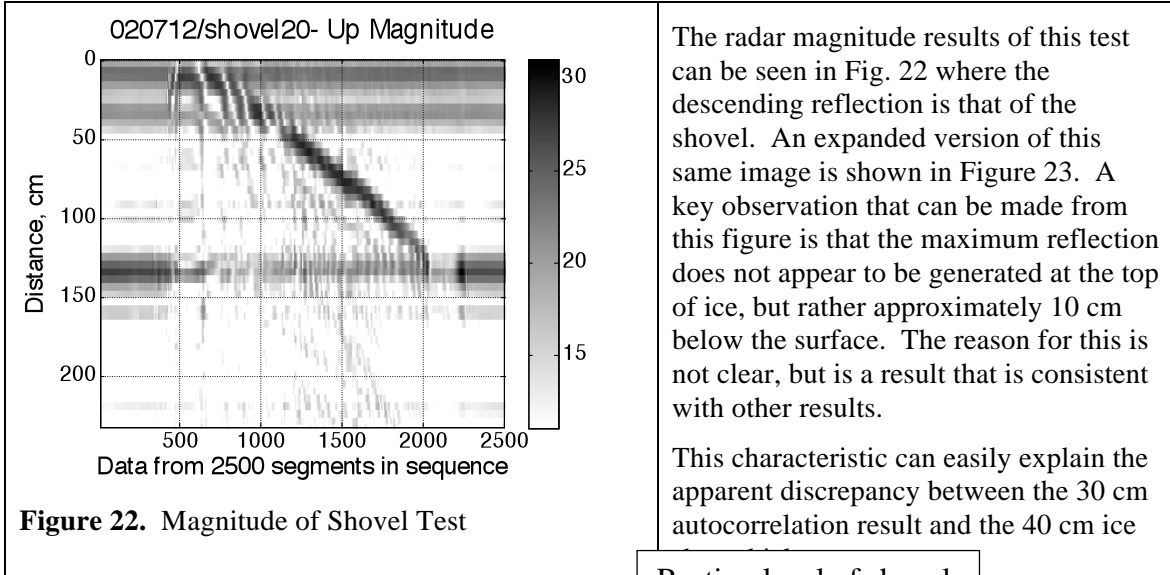
Figure 22. Magnitude of Shovel Test

The radar magnitude results of this test can be seen in Fig. 22 where the descending reflection is that of the shovel. An expanded version of this same image is shown in Figure 23. A key observation that can be made from this figure is that the maximum reflection does not appear to be generated at the top of ice, but rather approximately 10 cm below the surface. The reason for this is not clear, but is a result that is consistent with other results.

This characteristic can easily explain the apparent discrepancy between the 30 cm autocorrelation result and the 40 cm ice

Figure 23. Expanded Magnitude of Shovel Test

Another way to view the ice sheet is with the use of composite sweeps of magnitude and phase. These are shown in Figure 24 with the expanded version in Figure 25. The important parts of these plots are those outlined as the region of the ice sheet. The signals outside the ice sheet region are either the result of spurious signals or multiple reflections within the ice sheet. More study and system improvements will help to understand and/or eliminate these. It is also clear from these plots that a phase signal will always be present but has no significance in regions where the magnitude is very low.

Looking at the expanded signal in Figure 25, it is apparent that the magnitude of the reflection begins to increase at a distance of 110 – 115 cm below the bottom of the antennas (note that this distance is computed based on the assumed dielectric constant for the ice (4.5 in this case) so that the indicated distance to the top of ice in air would be around 245 cm. Refinement in the analysis offset variable to estimate the true bottom of the horns would probably add about 30 cm to this distance.

The differential phase is calculated as the slope in the phase vs. distance after the expected constant phase vs. distance is subtracted. Thus this parameter provides an estimate of the change in the phase of the reflection at the reflecting surface. Both the magnitude and the phase signature of the ice seen in Figure 25 seem to be very typical of this ice sheet in most of the data. The reflection magnitude tends to peak approximately 10-20 cm after the apparent top of ice. The differential phase typically increases as the ice is penetrated, then is nearly constant with a slight trough, which is at a minima near the maximum magnitude.
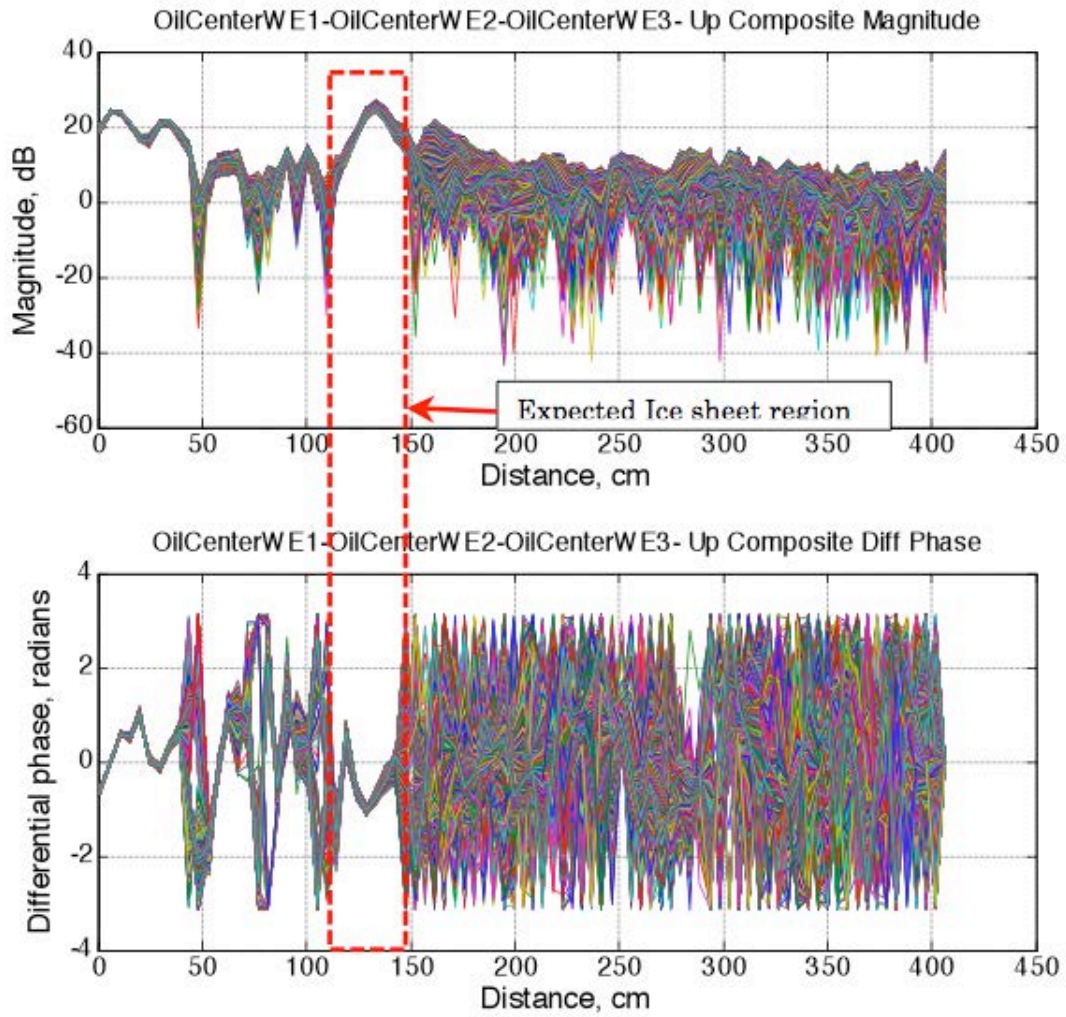
Figure 24. Typical Composite Magnitude and Differential Phase (5961 Segments)

More study of these magnitude and phase signatures for various combinations of ice temperatures and salinity could be very beneficial. Having a catalog of these signatures might enable the synergistic use of these signatures to better understand what to look for to determine the presence of oil under the ice.
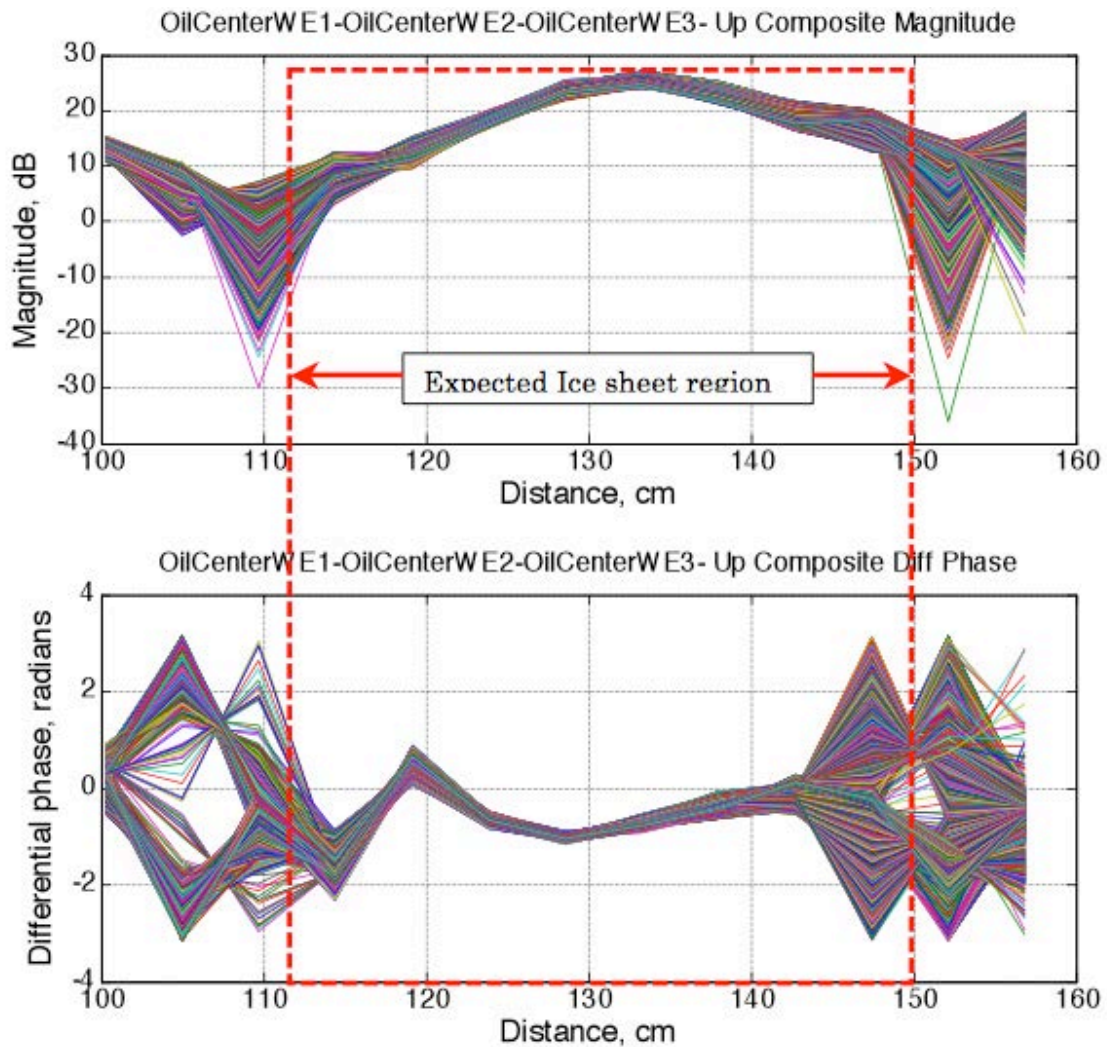
Figure 25. Expanded View of Typical Composite Magnitude and Differential Phase (5961
Segments)

Where's the oil?

Detecting the presence of oil under the ice is a considerable challenge, and with the data
collected at CRREL and the analysis done so far it is not clear whether the oil was
visible. Perhaps the most interesting data is that was collected during the oil discharge
itself. This data is somewhat confounded by different ice conditions during the two days
and the warming of the ice surface during the second day. However, there are some
interesting observations that might be made. As noted above, the ice layer had the
characteristic of being apparently non-homogeneous and therefore reflecting the radar
signal throughout its thickness. It would be reasonable to expect that an oil layer would
tend to be reasonably homogeneous and therefore create reflections at the interfaces but
relatively little within the layer.

The magnitude data collected during the 2-day oil spill is shown in Figure 26. The top
of this figure is at the approximate top of ice, and it can be seen that there is a region

starting at about 152 cm where the magnitude of reflection is very low. Unfortunately, there appears to be little from this plot that shows a significant change due to the increasing thickness of oil under the ice. There are some step changes that happened at around segment 2200, which is the boundary between the two days of testing. This could be attributed to the change in ice conditions over night or to possible changes in the gantry position between the two tests.
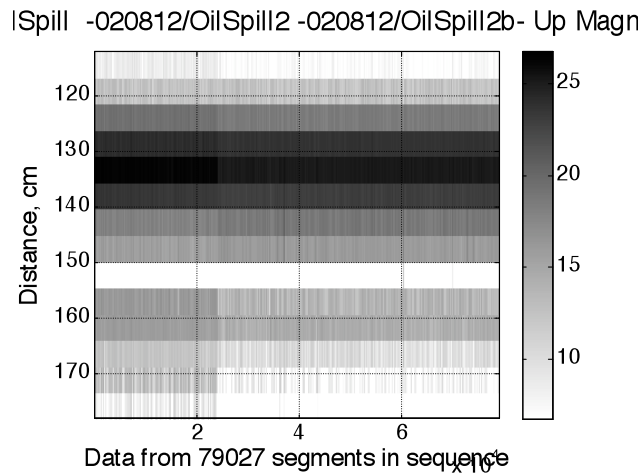

Figure 26. Reflection Magnitude during Oil Spill

Further information appears to be revealed by the phase data. From Figure 27 there are some apparent shifts in the levels just above and just below 150 cm. A look at the phase from the level just below 150 cm is shown in Figure 28, where the red curve is based on the best-fit second order approximation. The data shown in Figure 28 is clearly very noisy, as it is coming from a region with a small magnitude of reflection. However, the smoothed data is changing by nearly 0.5 radians, which is a significant change. Developing a way to detect this phase shift while flying over the ice will require more analysis of data collected from testing in a well-controlled environment.
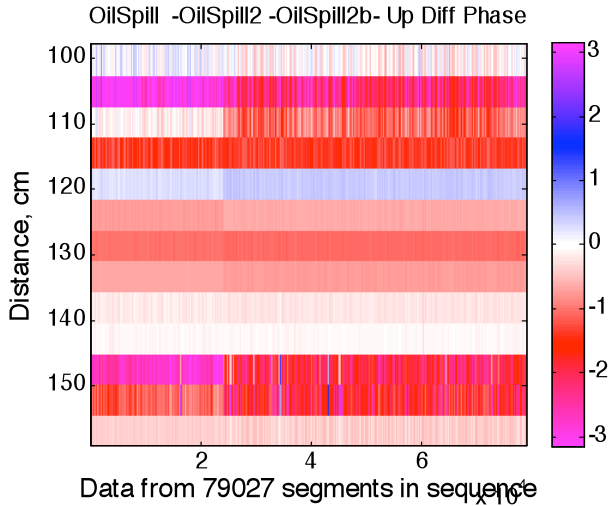
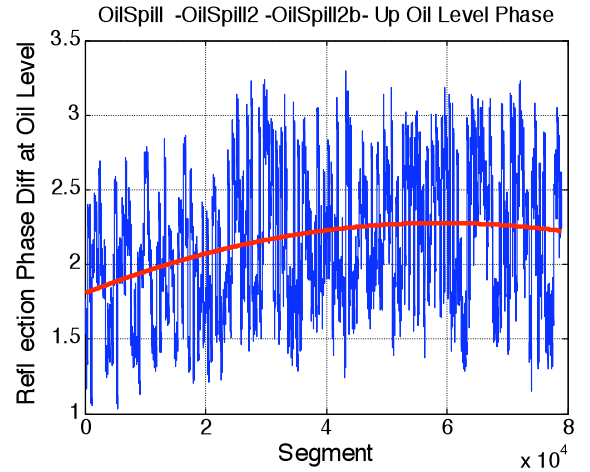**Figure 27.** Diff Phase for Ice Sheet during Spill

Figure 28. Phase Trend detected during Oil Spill

Another example presented in investigating the possible detection of oil is shown in Figure 29. This plot is the result of moving the gantry from west to east near the north end of the pool, with the north/south position chosen so that the radar would cross the center of the oil spill. The center of the scan would then be expected to be in the oil spill region. Note that this region also included a thinner section of ice, the ice depression shown in Fig. 6, which could also contribute to the results. The rate of traversing across the center section was much slower than across the west or east portions, so the amount of time spent over the oil region would be larger than the area represented by that region.
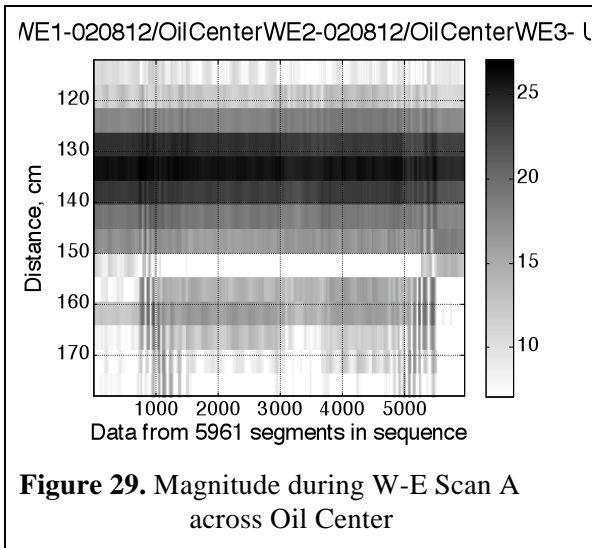
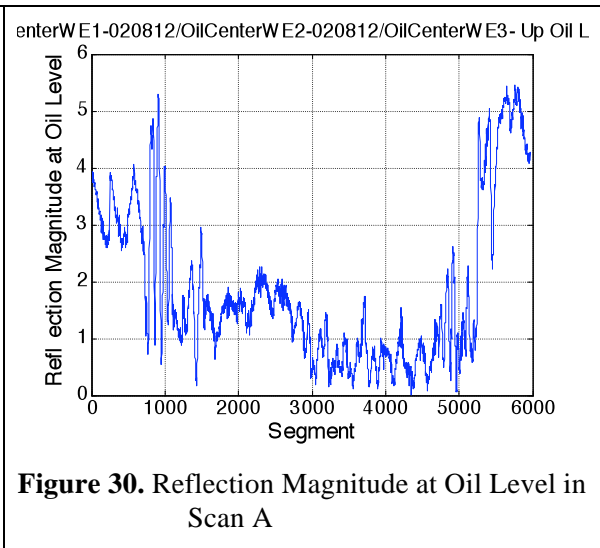**Figure 29.** Magnitude during W-E Scan A across Oil Center

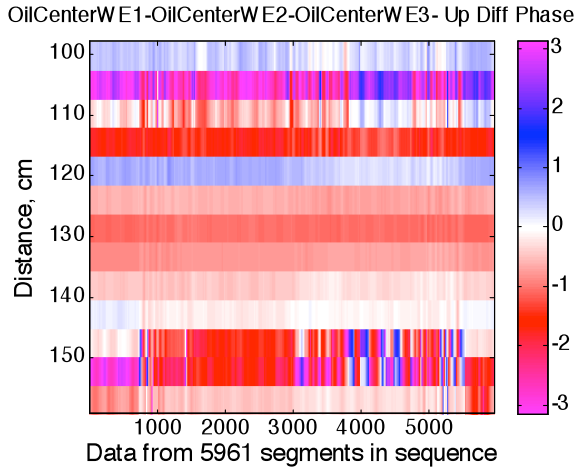**Figure 30.** Reflection Magnitude at Oil Level in Scan A

Figure 31. Differential Phase during W-E Scan across Oil Center

The differential phase plot is shown in Figure 31. While the interpretation of this plot will require more insight, it does appear that changes are happening at the expected oil level around 150 cm.

It would be premature to say with certainty that the observed trends were caused by the oil level under the sheet. The signals are weak and the signatures are only guesses without supporting data, but there is reason to be encouraged that detection may be feasible even with the close to melting ice available for the tests.

Two other W-E scans were done across the oil spill center of the pool. One, referred to as Scan B, showed similar magnitude and phase results to the ones shown in Figure 29 through Figure 31. The other scan, referred to as Scan X, with the antenna pair rotated by 90 degrees, showed very different results. These results can be seen in Figures 32 to 39.
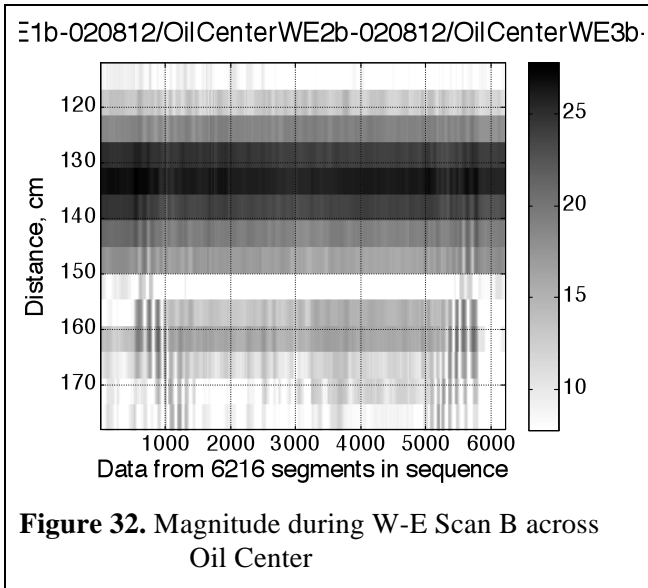

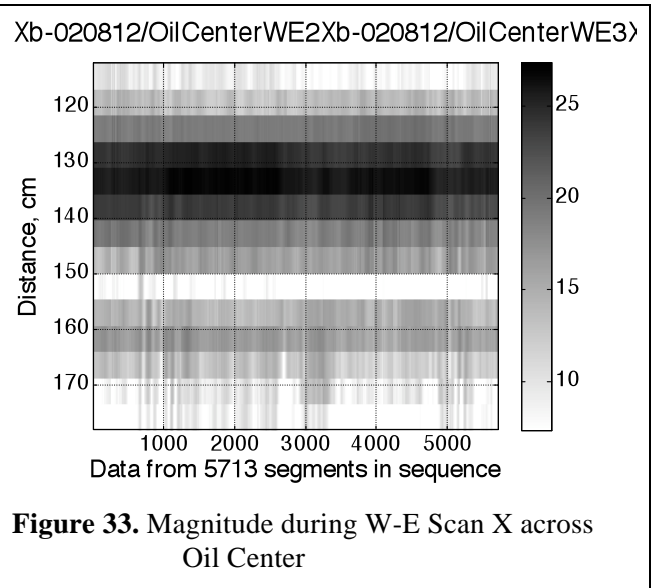
**Figure 32.** Magnitude during W-E Scan B across Oil Center

Figure 33. Magnitude during W-E Scan X across Oil Center

Figure 34. Reflection Magnitude at Oil Level in Scan B

Figure 35. Reflection Magnitude at Oil Level in Scan X

Figure 36. Phase during W-E Scan B across oil center.

Figure 37. Phase during W-E Scan X across oil center.

Figure 38. Phase at oil level during W-E Scan B across oil center.

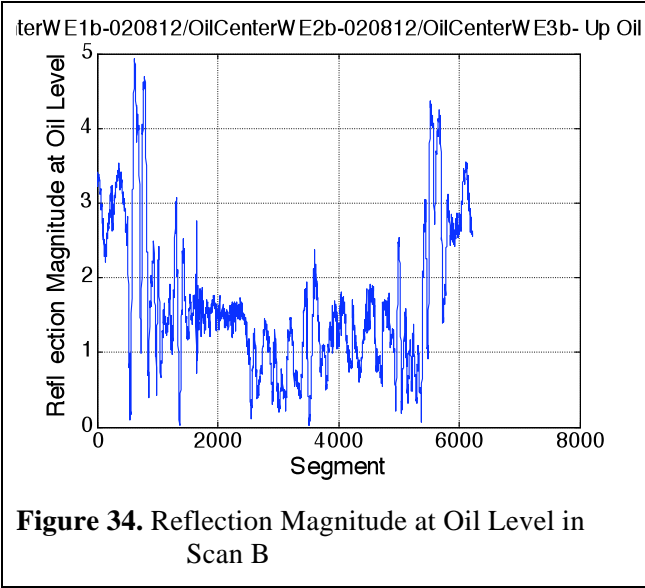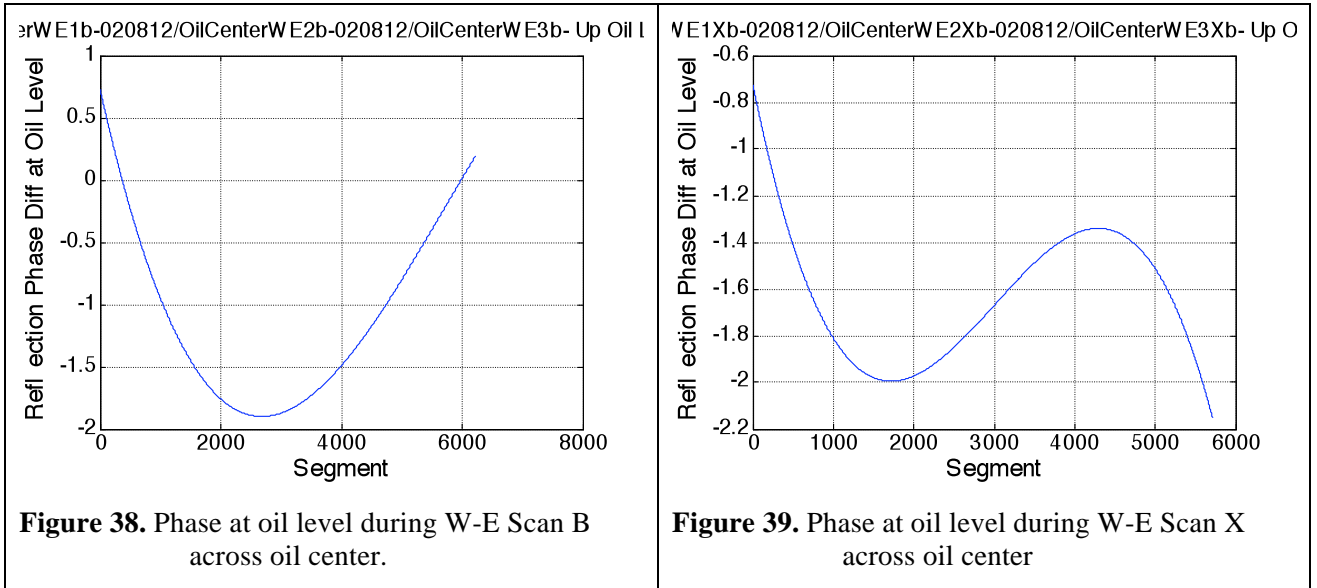**Figure 39.** Phase at oil level during W-E Scan X across oil center
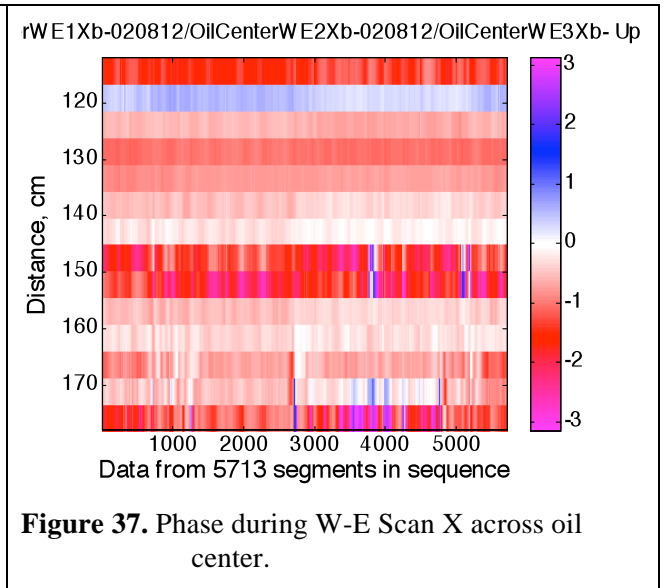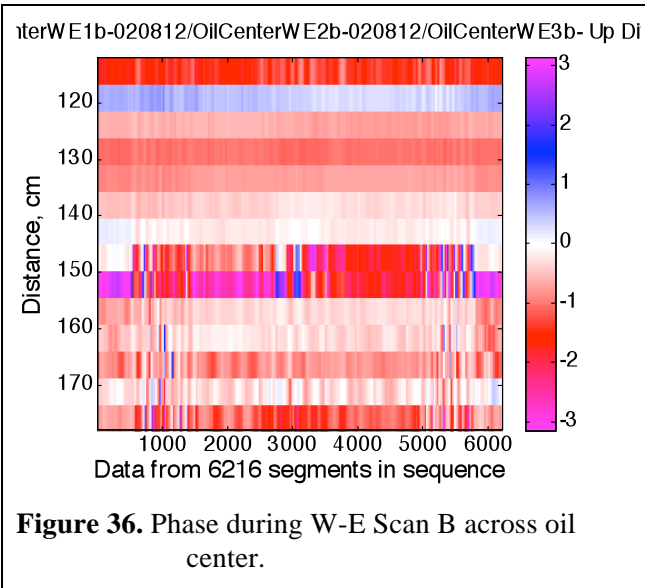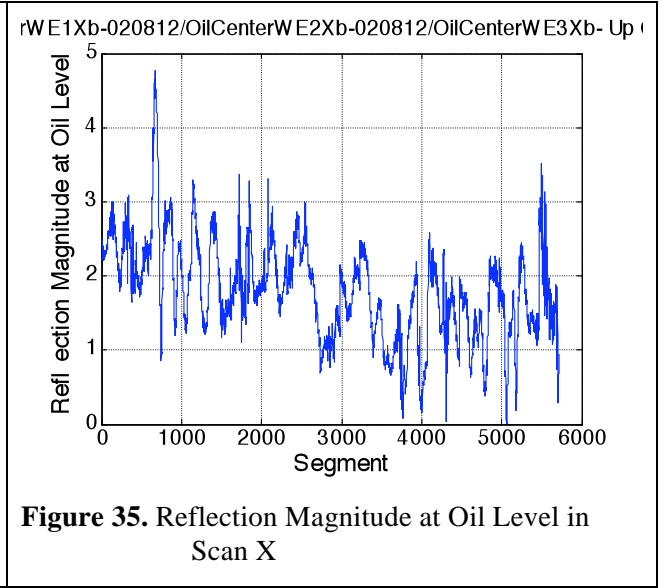
These experimental results supports the notion that the ice layer is not isotropic and confirm previous observations that field orientation of the antennae is important in acquiring the data.